Journal of Materials Chemistry A

RSC Publishing

PAPER

View Article Online
View Journal | View Issue

Cite this: J. Mater. Chem. A, 2013, 1, 9689

Cobalt doped $LaSrTiO_{3-\delta}$ as an anode catalyst: effect of Co nanoparticle precipitation on SOFCs operating on H_2S-containing hydrogen

Shao-Hua Cui,[ab] Jian-Hui Li,[bc] Xin-Wen Zhou,[b] Guang-Ya Wang,[b] Jing-Li Luo,*[b] Karl T. Chuang,[b] Yang Bai[a] and Li-Jie Qiao[a]

Received 1st April 2013
Accepted 10th June 2013

DOI: 10.1039/c3ta11315a

www.rsc.org/MaterialsA

This article compares the effects of Co doping on phase structures and stability of lanthanum strontium titanate (LST) anodes and electrochemical measurements in solid oxide fuel cells (SOFCs) employing H_2S-containing H_2 as fuel. The Co-doped LST (LSCT) with a perovskite structure was synthesized *via* a solid state approach, achieving excellent phase purity and refined particle size. The catalytic activity and electrochemical performance are significantly improved by introducing Co. A maximum power density of 300 mW cm^{-2} was achieved at 900 °C with 5000 ppm H_2S–H_2 in a fuel cell having a 300 μm thick YSZ electrolyte. Trace amounts of metallic Co nanoparticles with sizes typically no larger than 10 nm in diameter were detected on the LSCT surface after reduction in H_2 at 900 °C. The nano-sized Co clusters could reduce the anode polarization resistance, as well as improve the cell performance, compared with undoped LST anodes. The LSCT anode catalyst was electrochemically stable in 5000 ppm H_2S–H_2 during the test time at high operating temperature. The LSCT anode catalyst also had relatively high redox stability in reversible oxidation–reduction cycles.

1 Introduction

Solid oxide fuel cells (SOFCs) have received extensive attention in recent years as they can be used for high efficiency power generation with environmental friendliness and fuel flexibility.[1] They can operate on a variety of oxidizable fuels, including syngas, natural gas and other hydrocarbons other than pure hydrogen.[2] Direct utilization of hydrocarbons as the fuel becomes much more attractive due to their natural abundance, cost effectiveness, ease of storage and transportation compared to pure hydrogen. However, several prospective anode materials encounter serious degradation when operating under hydrocarbon fuels due to carbon deposition and hydrogen sulfide (H_2S) poisoning, resulting in toxic contamination and corrosion issues on the entire system.

The conventional Ni-based anode material, which is very active in H_2 oxidation, is not suitable to be employed under sulfide-containing conditions, since it reacts rapidly with H_2S to form nickel sulphide and poisons the catalyst surface, even at low H_2S concentrations.[3,4] A number of studies have been carried out to design alternative anodes that can endure harsh environments. Perovskite structure materials are promising Ni-free anode candidates based on their high chemical stability, strong resistance to carbon deposition and sulfur poisoning.[5] Among the variety of perovskite materials, including titanate-based, chromite-based, vanadate-based perovskite materials and double perovskite materials, lanthanum strontium titanate ($La_xSr_{1-x}TiO_{3-\delta}$, LST) is much attractive due to its thermal and chemical stability under the reducing conditions in the presence of H_2S.[6] However, this material suffers from a relatively low catalytic activity of the fuel oxidation reactions.

For the improvement of LST-based anode materials, much research has been conducted in this field, following three main directions: (1) developing new methods to obtain LST-based anode nano-structured materials; (2) combining LST with other nano-structured materials such as cermet, oxide or metal; (3) doping LST with appropriate elements in different sites with different quantities. The electronic and/or ionic conductivity, as well as stability, can be improved by the introduction of different dopants such as Ce,[7] Ca,[8] Co[9] or other elements ($La_{0.33}Sr_{0.67}Ti_{0.92}X_{0.08}O_{3-\delta}$, X = Al^{3+}, Ga^{3+}, Fe^{n+}, Mg^{2+}, Mn^{n+}, and Sc^{3+}).[10] The catalytic activation for hydrogen oxidation can be greatly enhanced by doping with cobalt because of a high capability for hydrogen dissociation. In fact, Co-based catalysts have been widely used in hydrogen-related reactions, such as the Fischer–Tropsch reaction,[11] the hydrogenation of aromatic compounds,[12] and the selective hydrogenation of aldehydes.[13] The effect of Co-doping on the electrical behaviour of

[a]Corrosion and Protection Center, Key Laboratory for Environmental Fracture (MOE), University of Science and Technology Beijing, Beijing, 100083, China

[b]Department of Chemical and Materials Engineering, University of Alberta, Edmonton, Alberta, T6G 2G6, Canada. E-mail: jingli.luo@ualberta.ca; Fax: +1-780-492-2881; Tel: +1-780-492-2232

[c]National Engineering Laboratory for Green Chemical Productions of Alcohols–Ethers–Esters, College of Chemistry and Chemical Engineering, Xiamen University, Xiamen, 361005, China

$La_{0.3}Sr_{0.7}TiO_{3-\delta}$[9] and $Y_{0.08}Sr_{0.92}TiO_{3-\delta}$[14] has been carefully investigated. The results showed that the electrical conductivity of doped samples decreased with increasing Co-doping amount, which could be ascribed to the lowered Ti^{3+} concentration. At the same time, the ionic conductivities increased significantly at high temperature due to the increase of oxygen vacancy and concentration and enlargement of the saddle point critical radius r_c.

Nanostructured materials are anticipated to be adapted in SOFC electrodes because of the dramatically increased surface areas and the triple-phase boundary (TPB) lengths which result in a significantly improved cell performance.[15] It has been reported[16,17] that high performance SOFCs were achieved with nanostructured electrodes by a wet infiltration method. However, the inevitable agglomeration and grain growth of the nanoparticles led to the performance degradation as well as poor redox stability during the long-term fuel cell operation.[16,17] Barnett's group, for the first time, found a method of forming catalytic metal nanoparticles *in situ via* ex-solution from the perovskite oxide host in a reducing environment. They studied Ni- and Ru-doped chromite perovskite materials, and observed that the nanoclusters of metallic Ni or Ru precipitated onto the $La_{0.8}Sr_{0.2}Cr_{1-y}X_yO_{3-\delta}$ (X = Ni, Ru) surface upon reduction.[18–20] According to the paradigm that Barnett's group proposed, Gorte's group has recently shown that the transition metal nanoparticles (Ni, Co, and Cu) could be moved out of and into the transition metal-doped vanadate ($Ce_{1-x}TM_xVO_{4-0.5x}$, TM = Ni, Co, Cu) lattices by redox cycling.[21]

In this work, the LST-based anode catalysts doped with Co have been studied and the catalytic behaviour of Co nanoparticles formed during reduction has been discussed. $La_{0.3}Sr_{0.7}Co_{0.07}Ti_{0.93}O_{3-\delta}$ (LSCT) was employed as the anode catalyst in SOFCs fuelled by both H_2 and 5000 ppm H_2S–H_2 since the solid solubility limitation of Co in LST at 1500 °C was about 7 mol% at which the highest ionic conductivity was shown in a series of compounds with different Co ratios.[9] The stability and electrochemical properties of this anode material were investigated for various fuels. The reversible oxidation–reduction behavior was also measured. The thermodynamic calculation using HSC 5.1 Chemistry software was performed to identify the equilibrium composition using 5000 ppm H_2S–H_2 as the fuel.

2 Experimental

2.1 Catalyst preparation

$La_{0.3}Sr_{0.7}TiO_{3-\delta}$ and $La_{0.3}Sr_{0.7}Co_{0.07}Ti_{0.93}O_{3-\delta}$ catalyst powders were prepared using solid state synthesis. Initially, stoichiometric amounts of high purity La_2O_3 (Alfa Aesar, 99.99%), TiO_2 (BDH, 99.5%), $SrCO_3$ (Fisher, 99%) and Co_3O_4 (BDH, 99.5%) powdered precursors were ball milled for 12 h, followed by calcining the mixture in air at 1000 °C for 4 h. The resulting powders were subsequently ball milled for 5 h, and pressed uniaxially at a low pressure to form pellets and then calcined in air at 1300 °C for 5 h. The final powders were reduced in 10% H_2–N_2 (Praxair) at 1400 °C for 10 h. Commercial YSZ powders (TOSHO) were used without any pre-treatments.

2.2 Fuel cell fabrication

Fuel cells were fabricated using commercial YSZ disks (Fuel Cell Materials) as electrolytes, 300 μm in thickness and 25 mm in diameter. Both the anode and cathode were intimate mixtures of equal mass of LST and YSZ powders with a pore former – polymethyl methacrylate (PMMA). Alternatively, LSCT perovskite catalysts were also used as the anode, and commercial strontium doped lanthanum manganite (LSM) as the cathode, respectively. The mixtures mentioned above were finely powdered in a planetary ball milling. The electrode inks were prepared by mixing the powders with α-terpineol (Alfa Aesar): isopropanol = 2 : 1 as a solution containing 5 wt% poly(vinyl butyral-*co*-vinyl alcohol-*co*-vinyl acetate) (PVB, M_w = 70 000–100 000, Aldrich) and 5 wt% ethyl cellulose (Aldrich). Each electrode ink was screen printed onto the corresponding face of the electrolyte to form a membrane electrode assembly (MEA) with a circular area of 1 cm^2, and then presintered in air at 1200 °C for 1 h. After the MEA was sintered, 1 cm^2 gold and platinum pastes were painted onto the sides of the anode and cathode, respectively, which were then sintered *in situ* to form current collectors. There was an annular blank area between the electrode zone and the edge of the electrolyte disk.

2.3 Fuel cell testing

The MEA was placed between two coaxial alumina tubes (inlet and outlet) to form the anode and cathode compartments. Gold current collector wires with spiral wound ends ran through the length of the inner tube. Fuel cell tests were conducted using a four-electrode setup. A glass sealant (Ceramabond, Aremco Products) was applied to seal the outer tube (outlet) directly to the outer edge of the anode side of the single cell electrolyte. The cell was then heated in a Thermolyne F79300 tubular furnace. Before all single cell tests, the anodes were reduced *in situ* at 900 °C. The cathode side of each MEA was not sealed within a tube, and its compartment was supplied with an air flow of 75 mL min^{-1}. Pure hydrogen (H_2, Praxair) or hydrogen mixed with 5000 ppm hydrogen sulfide (0.5% H_2S–H_2, Praxair) was used as fuel and fed at a rate of 75 mL min^{-1}. Before measurements, the system was stabilized after each change of temperature and feed. Fuel cell testing was performed with standard DC and AC electrochemical techniques using a Solartron instrument (SI1287 EI). The polarization resistance of the cell was measured using electrochemical impedance spectroscopy (EIS) that was controlled by *Z*-plot electrochemical impedance software over the frequency range from 1 MHz to 0.1 Hz at open circuit voltage (OCV).

2.4 Chemical stability testing

Chemical stability tests were conducted using the powders of anode materials, which were put in an alumina boat placed in a quartz tube. The samples were heated to 900 °C in a stream of flowing 10% H_2–N_2 (Praxair), held at that temperature in 5000 ppm H_2S–H_2 (Praxair) for 48 h, and then cooled down to room temperature under flowing 10% H_2–N_2 again.

2.5 Redox tolerant testing

A series of redox cycles on LSCT were performed at 850 °C, with each redox cycle having the following steps: (1) flushing with highly pure nitrogen-steam for 5 min to fully eliminate the H_2; (2) switching off the anode gas supply and exposing the anode to ambient air for 30 min; (3) flushing with nitrogen-steam for 5 min again to fully eliminate the air; (4) reduction in H_2 until the cell reached a steady state. The measurements were taken after equilibrating the cell in H_2.

2.6 Material characterization

A RIGAKU RU-200B Rotating anode X-ray diffraction (XRD) system with a Cu target was used to analyze the phase composition of all synthesized powders at a scan rate of 2° min^{-1}. The commercial software Jade® 5.0 was used to identify the phase structure.

X-ray photoelectron spectroscopy (XPS) was performed using a Kratos Analytical AXIS 165. A monochromatic Al Kα source ($h\nu$ = 1486.6 eV) was used at a power of 210 W, with a base pressure of 3×10^{-8} Pa in the analytical chamber. Spectra were referenced to a C 1s binding energy of 284.8 eV, and were fitted using Gaussian–Lorentzian peak shapes and Shirley baselines.

A Vega-3 (Tescan, USA) scanning electron microscope (SEM) with a EDS detector (INCA, Oxford Instruments) was used to characterize the morphology and the element composition of the anode and the MEAs. Field emission scanning electron microscopy (FESEM) studies were carried out on the powder samples using a JAMP-9500F operated at 15 kV. Samples were coated by 2 nm of chromium and stored in a vacuum before FESEM measurements.

An FEI F-20 transmission electron microscope (TEM) was used to examine the LSCT powders after reduction in 10% H_2–N_2 at 1400 °C for 10 h. The powders were dispersed in alcohol using sonication. A drop of the suspension was deposited on a carbon-coated TEM Cu grid. The samples were dried in air before TEM characterization.

3 Results and discussion

3.1 Structural characterization

3.1.1 Catalyst phase and microstructure characterization. Fig. 1a shows the typical XRD patterns of the as-prepared LSCT powder, reduced in 10% H_2–N_2 at 1400 °C for 10 h, and pre-treated in 5000 ppm H_2S–H_2 at 900 °C for 48 h, respectively. The main peaks matched those of the standard $SrTiO_3$ perovskite structure (PDF #05-0634), indicating that each of the tested materials has a cubic perovskite structure. This behaviour is expected for a solid solution when the cationic substitution does not change the structure. After reduction in 10% H_2–N_2 or treatment in 5000 ppm H_2S–H_2, trace amounts of precipitated metallic Co as well as a small systematic shift in the peak positions were observed (Fig. 1b). In this study, the perovskite structure of LSCT was maintained after treatment although the ex-solved Co nanoparticles were observed. This observation is consistent with the results reported in ref. 18 and 21, where the metal nanoparticles precipitated onto the oxide surface had

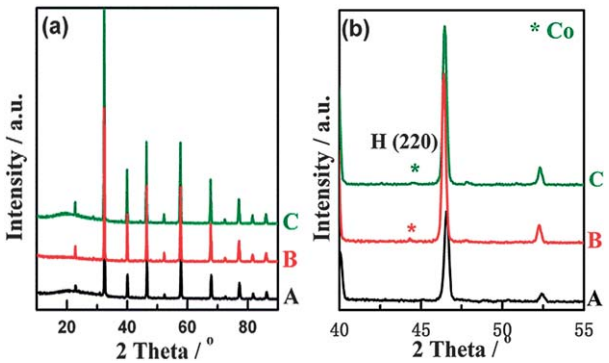

Fig. 1 (a) XRD patterns of the LSCT samples: (A) as-prepared, (B) reduced in 10% H_2–N_2 at 1400 °C for 10 h, and (C) treated in 5000 ppm H_2S–H_2 at 900 °C for 48 h; (b) magnified view of A.

negligible influence on the crystalline phase structure upon reduction.

In addition, the width of the peaks corresponding to hexagonal close-packed (220) of Co was broad, indicating that the size of the precipitated metallic Co particles was quite small.[22] Actually, the crystallite sizes of the Co particles were calculated by the Scherrer formula ($L = 0.89\lambda/\beta\cos\theta$) from the line broadening of the (220) diffraction peak and the values were smaller than 10 nm.

Fig. 2 shows the SEM images of the as-prepared LSCT particles and those reduced in 10% H_2–N_2 at 1400 °C for 10 h. It can be seen that the surface of the as-prepared sample is quite clean without any nanoparticles on it (Fig. 2a). However, some small particles of ~10 nm diameter, corresponding to XRD characterization, can be observed on the reduced sample's surface (Fig. 2b). Generally, nanocatalytic materials with a small particle size should have better catalytic performance due to their high proportion of edge and corner atoms which are conventionally considered as active sites for adsorption of reactants. The ex-solved Co particles with small size may act as high active sites for hydrogen oxidation during the cell operation.

TEM images obtained from the reduced LSCT powders are shown in Fig. 3. After reduction in 10% H_2–N_2, hemispherical Co nanoparticles with diameters smaller than 10 nm were found (Fig. 3a). Nanoparticle lattice fringes (shown in Fig. 3b) yield atomic spacings along the (220) direction of 2.0 Å, which is

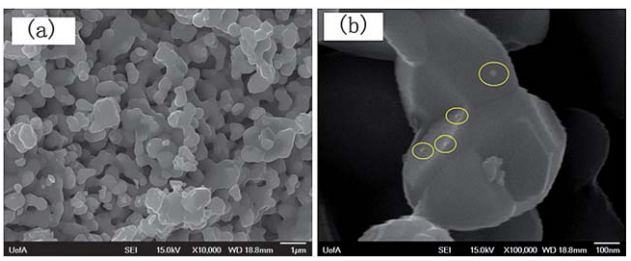

Fig. 2 SEM images of the LSCT samples: (a) as-prepared and (b) reduced in 10% H_2–N_2 at 1400 °C for 10 h.

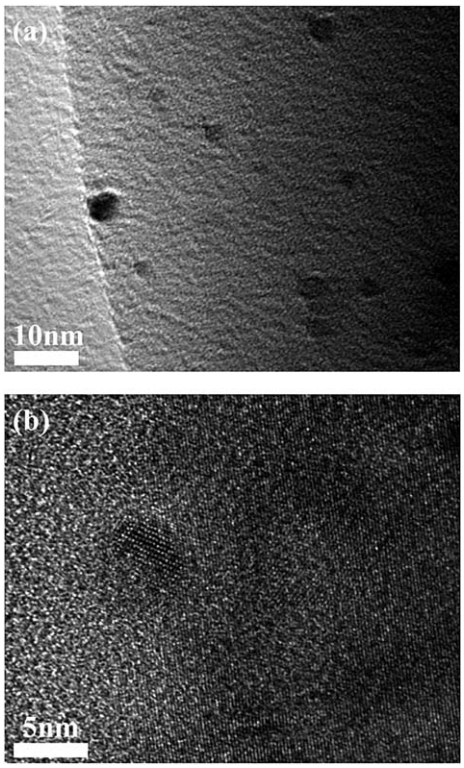

Fig. 3 (a) TEM images of the LSCT samples treated in 10% H_2–N_2 at 1400 °C for 10 h and (b) HR-TEM image.

in agreement with the reported value for hexagonal Co [PDF#65-9722]. The size and density of the Co particles in Fig. 3 are consistent with the XRD result and the SEM image (Fig. 2) under the same pretreatment.

3.1.2 Fuel cell characterization. Fig. 4a shows a typical EDS spectrum taken from the anode surface and all the elements for LSCT–YSZ can be observed on the surface. Fig. 4b–d are EDS maps obtained from the La Kα_1, Zr Kα_1, and Co Kα_1 peaks, respectively. The distribution of La and Zr indicated that the LSCT and YSZ particles were mixed uniformly and homogenously. The anode was formed by the firm connection of the composites with an average diameter of about 1 μm. In addition, Co distributed uniformly in the lanthanum strontium titanate lattice as expected.

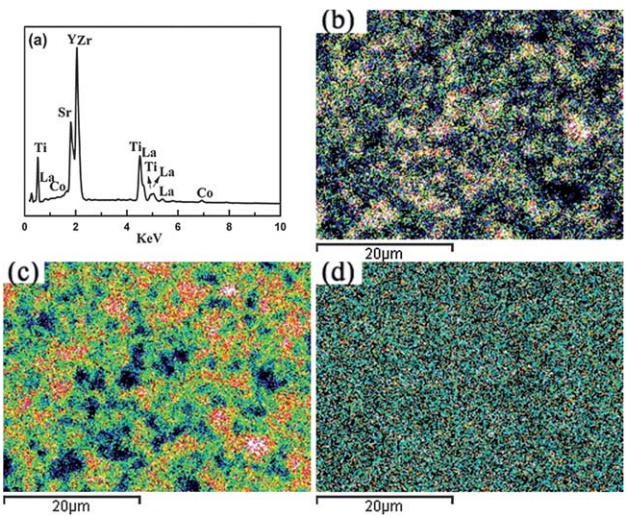

Fig. 4 (a) EDS spectrum and element maps of (b) La, (c) Zr and (d) Co.

Fig. 5 is a SEM image showing the fracture cross-section of a MEA. The thickness of the anode and the cathode is about 50 and 20 μm, respectively. A good contact between the porous electrode and the fairly dense electrolyte is seen in the SEM image.

3.2 Electrochemical analysis

3.2.1 Electrochemical performance. Potentiodynamic tests were conducted to determine the electrochemical activity of the anode material for conversion of both H_2 and H_2S. The MEAs were tested at 800 °C, 850 °C and 900 °C, respectively, using pure H_2 and 5000 ppm H_2S–H_2. All the electrochemical data were obtained only after the cell had reached a steady state. Fig. 6 compares the maximum power densities of both anode catalysts obtained in different feeds and at different temperatures. In pure H_2, the power density increased with temperature for both LST and LSCT-based cells (Fig. 6a). Both anode catalysts were active for the conversion of H_2, and the Co substitution significantly improved the cell performance. The maximum power density of the LSCT-based cell was 230 mW cm^{-2} in H_2 at 900 °C, which was more than twice higher than 90 mW cm^{-2}, obtained from the LST-based cell. Notably, obvious improvement in power density was observed for both cells when the feed

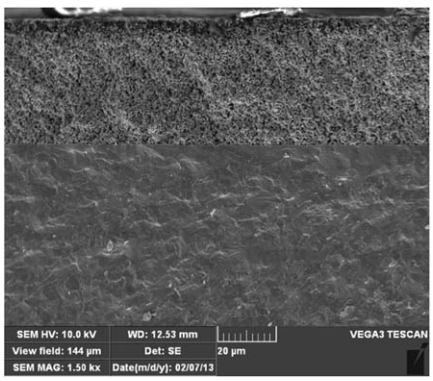

Fig. 5 Fracture cross-sectional view of a typical cell before testing.

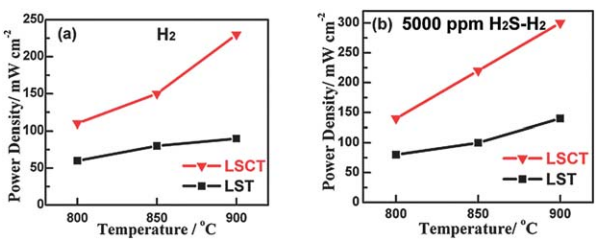

Fig. 6 Maximum power density of the cells with different fuels: (a) pure H_2 and (b) 5000 ppm H_2S–H_2 at different temperatures.

changed to 5000 ppm H_2S–H_2 (Fig. 6b). The addition of H_2S enhanced the anode's activity and provided better cell performance. The maximum power density of the LSCT-based cell was about 300 mW cm^{-2} in 5000 ppm H_2S–H_2 at 900 °C. For the LSCT-based cell, in both H_2 and H_2S-containing H_2, there was a stronger performance dependence on temperature with better performance when the temperature increased from 800 °C to 900 °C. Moreover, all the results have shown that LSCT exhibited a much better performance than LST under the same test conditions.

Detailed *I–V* and *I–P* curves for LSCT-based cells using both H_2 and 5000 ppm H_2S–H_2 as feeds are compared in Fig. 7. As expected, the peak power density improved as the temperature increased from 800 °C to 900 °C in both feeds. The maximum power density of the LSCT-based cell tested in 0.5% H_2S–H_2 at 900 °C was about 300 mW cm^{-2} at a current density close to 500 mA cm^{-2} and a potential of 0.6 V (Fig. 7b), which is obviously larger than that in pure H_2.

3.2.2 Electrochemical impedance spectroscopy. Fig. 8a shows the corresponding electrochemical impedance spectra for both LST-based and LSCT-based cells using H_2 as fuel under OCV conditions at 900 °C. These spectra were obtained after stabilization of the cell performance. The ohmic resistances determined from the high-frequency intercepts with the real axis in the Nyquist plot were similar for both cells. However, the polarization resistance of both cells was definitely different. The measured polarization resistance was evidently dropped by Co-doping, according to the previous reports[23] that the absorbability of H_2 onto the perovskite oxide surface was correlated with the reducibility of B site ions. Hence, the performance of the LSCT-based cell is better than the LST-based cell in H_2 (Fig. 6a), which may originate from the higher reducibility of Co than Ti.[24] In addition, the reduced LSCT catalyst with precipitated Co nanoparticles had a high catalytic activity since the nano-structured anode catalyst can dramatically improve the cell performance by increasing the concentration of TPB sites.

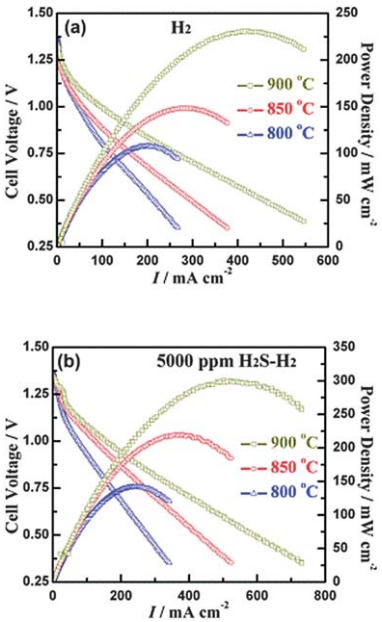

Fig. 7 Current density–voltage and power density curves of LSCT-based cells at different temperatures (a) in pure H_2 and (b) in 5000 ppm H_2S–H_2.

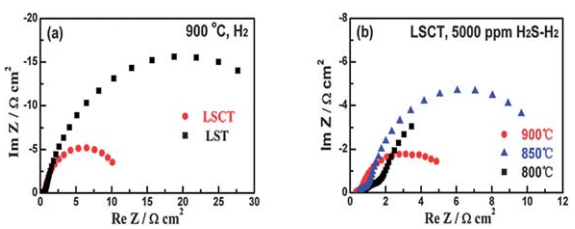

Fig. 8 Impedance spectra of (a) both LST-based and LSCT-based cells fueled with H_2 at 900 °C and (b) LSCT-based cell fueled with 5000 ppm H_2S–H_2 at different temperatures.

Fig. 8b shows the corresponding electrochemical impedance spectra of the LSCT-based cell tested in the 5000 ppm H_2S–H_2 fuel at different temperatures under OCV conditions. Both the ohmic and polarization resistances are reduced with temperature, which corresponds to the *I–P* result shown in Fig. 7b. The activation polarization resistance of the LSCT-based cell measured in 5000 ppm H_2S-containing H_2 at 900 °C was about 0.35 Ω cm^2, which was only half of that in pure H_2, indicating that H_2S could promote the H_2 oxidation so that the cell performance improves.[25–27] The way that H_2S adsorbs on the anode surface seems to be a key in its promoting effects. On one side, the sulfur chemisorption on oxygen to obtain H_2–S–O is an easy process that even happens at room temperature, thus the energy gap to transfer the proton to the oxygen *via* H–S–O is smaller than that the one needed to break the H–H bond (which is actually quiet high). On the other side, sulfur (bond with oxygen or not) itself regenerates easily in H_2 to produce H_2S. Finally, H_2S is useful as it must be considered as a hydrogen carrier but its affinity with the surface oxygen is higher than pure H_2. However, the values of the concentration polarization resistance for both catalysts were high and could be decreased by optimizing the composition or the microstructure of the electrodes in future experiments.

3.3 Stability tests

3.3.1 Chemical stability. Chemical stability tests were performed to determine the sulfur tolerance of the catalysts in 5000 ppm H_2S–H_2 at 900 °C for 48 h. As shown in Fig. 1, treated LSCT powders retained the structure of the as-prepared materials, indicating that the LSCT catalyst was stable in these reducing and H_2S-rich environments.

XPS analysis was used to identify the near-surface composition and the ion electronic states of Co before and after the chemical stability tests. The LSCT catalyst after H_2 reduction and 5000 ppm H_2S–H_2 treatment for 48 h was compared. Fig. 9a shows the full range XPS binding energy spectra from both samples, while Fig. 9b shows the expanded region in the 775–805 eV range for the binding energy of Co species. The binding energy of all elements in the catalyst remained almost unchanged. However, after treatment in 5000 ppm H_2S–H_2, the

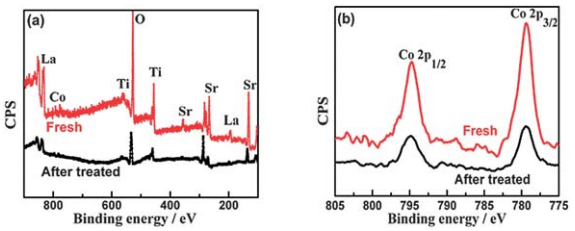

Fig. 9 XPS spectra of LSCT catalysts treated in H_2 and in 5000 ppm H_2S–H_2 for 48 h at 900 °C in (a) full range and (b) Co 2p binding energy region.

peak intensity of all the component elements decreased with the mass concentration of S increased from trace amount to 2%. It is well known that H_2S can decompose into hydrogen and elemental sulfur at high temperature, thus the LSCT surface was inevitably covered by sulfur, which would affect the intensity of XPS peaks. Both XPS and XRD showed that the oxide was stable in the high concentration H_2S-containing environment, indicating that LSCT is a good sulfur tolerant catalyst. However, since the analysis was performed *ex situ*, XPS and XRD results cannot entirely exclude the possibility of existence of the transient species that might be present during the operation of the fuel cell.

3.3.2 Electrochemical stability. The electrochemical stability test was performed with the LSCT-based cell in humid 5000 ppm H_2S–H_2 for 48 h at 900 °C at a fixed current density of 400 mA cm^{-2} (Fig. 10). No obvious degradation occurred within the long time frame, which is an indication that LSCT was electrochemically stable under these conditions. EDS spectra of the samples after reaction showed that no sulfur was deposited on the surface of the anode catalyst during stability tests. This showed that the LSCT anode catalyst was not prone to the problems associated with the use of Ni cermets in H_2S-containing fuel, and that the LSCT anodes exhibited good sulfur tolerance in SOFCs operated using H_2S-containing fuels. The high concentration of H_2S (5000 ppm) in the feed did not poison the catalyst and no sulfur was deposited on the anode.

3.3.3 Redox stability. Fig. 11 shows the maximum power density of the LSCT–YSZ anode during the 5 redox cycles. As seen in this figure, these reversible oxidation–reduction

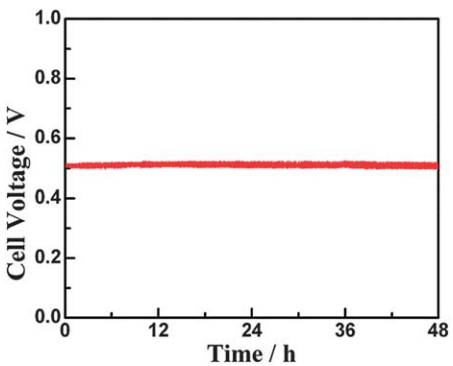

Fig. 10 Long-term stability test of the LSCT-based cell at 400 mA cm^{-2} and 900 °C in humid 5000 ppm H_2S–H_2 feed.

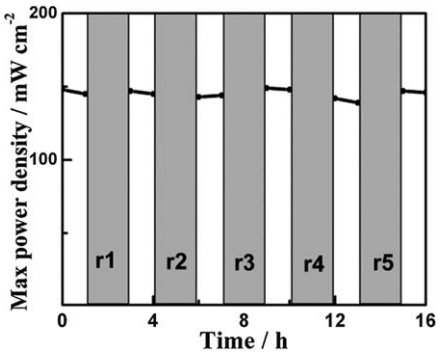

Fig. 11 Maximum power density of the LSCT-based cell as a function of time at 850 °C with H_2 fuel after each redox cycle.

treatments had no obvious adverse effect on the cell performance. The cell performance was found to remain relatively stable during multiple redox cycles.

The tolerance for repeated reduction and oxidation cycles is critical to the endurance of an anode in practical use. For example, under operating conditions, the cells generally suffer from a serious degradation as a result of catalytic metal nanoparticles coarsening. The agglomeration of the metal easily causes disconnection and a loss of TPB sites. However, this kind of degradation is recovered by a redox cycle, in which the metal is re-dissolved into the perovskite structure during the oxidation treatment, followed by metal nanoparticles being reproduced when the anode is reduced in H_2.[21] The high redox stability of LSCT may be due to the reversible moves of the metallic Co into and out of the perovskite lattice when exposed to the oxidizing and reducing conditions. Thus, the catalyst of this kind was able to refresh itself through the redox process and therefore was able to maintain its catalytic activity throughout the lifetime of a cell.

3.4 Thermodynamic analysis

In this work, it was demonstrated that a portion of metallic Co ex-solved from the LSCT lattice and formed Co nanoparticles on the surface of perovskite oxide upon reduction. Based on TPB theory, the precipitated Co nanoparticles can greatly improve the electron transfer channels and increase the concentration of TPB sites, thereby improve the whole anode performance. In a H_2S rich environment, Co easily reacts with H_2S to form CoS since Co is bivalent under these conditions.[24,28] However, CoS can also be reduced to Co by H_2:

$$Co\ (s) + H_2S\ (g) \leftrightarrow CoS\ (s) + H_2\ (g)$$

Hence, it is important to verify the existence of the forms of Co compounds in our testing environment (5000 ppm H_2S balanced with H_2). Although the metal sulfide can be used as the catalyst for the conversion of pure H_2S in SOFCs, its performance is poor due to the low catalytic activity. In addition, the performance obviously decreases during the long-term test probably due to the anode delamination.[29] Thus, it was

Table 1 Standard molar reaction Gibbs free energy and molecular reaction Gibbs free energy at different temperatures for the reaction

	800 °C	850 °C	900 °C
$\Delta_r G_m^{\theta}$ (kJ mol^{-1})	−36.441	−34.989	−33.547
$\Delta_r G_m$ (kJ mol^{-1})	14.318	17.304	20.458

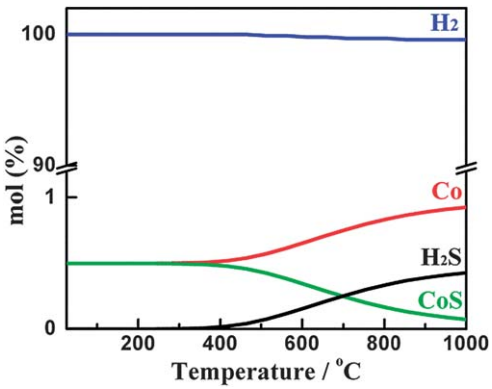

Fig. 12 Phase diagram of Co and CoS in 5000 ppm H_2S–H_2 as a function of temperature.

expected that the precipitated Co nanoparticles would be stable as metallic Co in this environment, since the catalytic activity of Co was much higher than that of cobalt sulfide for both H_2 and H_2S oxidation. Although the results from both XRD and XPS measurements showed that only metallic Co was detected after the fuel cell tests, the possibility of the existence of cobalt sulfide during fuel cell operation cannot be excluded, since the analyses were performed *ex situ*. A thermodynamic calculation using HSC 5.1 Chemistry software was performed to identify the equilibrium composition under these conditions.

The Gibbs free energy of the above reaction is obtained using the equilibrium composition at different temperatures according to the Van't Hoff equation The values reported in Table 1 are positive over the entire SOFC operating range from 800 °C to 900 °C. The Gibbs free energy increased with temperature, which means that reduction of CoS to Co by H_2 was more thermodynamically favourable at higher temperature. In these tests, the operating conditions of the cell were 5000 ppm H_2S balanced with H_2, therefore, the H_2 concentration was much higher than that of H_2S. It might be difficult to form CoS in such a condition because the H_2S concentration was lower than the requirement for sulfide formation.[3] Fig. 12 shows the phase diagram of Co and CoS in 5000 ppm H_2S–H_2 as a function of temperature. It is clear that starting from 400 °C, the amounts of Co and H_2S further increase with temperature, resulting in the decrease of CoS and H_2 amounts.

4 Conclusions

The effect of Co-doping on the catalytic activity and electrochemical behaviour of $LaSrTiO_{3-\delta}$ as an anode catalyst for SOFC fueled with H_2S-containing H_2 was investigated. A distinct phase of LSCT can be formed through synthesis by a solid state method. The XRD patterns and SEM images of the catalyst after reduction in hydrogen showed that the Co nanoparticles with diameter not larger than 10 nm were formed on the anode surface. These Co nano-clusters can increase the catalytic activation in fuel oxidation, which can reduce the anode polarization resistance and improve the cell performance. The maximum power density of the LSCT-based cell was about 300 mW cm^{-2} and no obvious degradation was detected during the galvanostatic test for 48 h in 5000 ppm H_2S–H_2 at 900 °C. In addition, no sulfur was deposited on the anode, showing good electrochemical stability of the Co-doped samples. Also, LSCT exhibited high redox stability which is critical to the endurance of the anode in practical uses. Therefore, LSCT proves to be a promising candidate for anode materials in SOFCs operating on H_2S-contaminated fuels.

Acknowledgements

This research was supported through funding to the Solid Oxide Fuel Cell Canada Strategic Research Network from NSERC and the National Nature Science Foundation of China under grant 51072021. The authors gratefully acknowledge financial support from China Scholarship Council. We would also like to thank Ying-Jie Yan for TEM analysis.

Notes and references

1 E. P. Murray, T. Tsai and S. A. Barnett, *Nature*, 1999, **400**, 649–651.
2 C. M. Grgicak, R. G. Green, G. Richard and J. B. Giorgi, *J. Power Sources*, 2008, **179**, 317–328.
3 A. Lussier, S. Sofie, J. Dvorak and Y. U. Idzerda, *Int. J. Hydrogen Energy*, 2008, **33**, 3945–3951.
4 S. W. Zha, Z. Cheng and M. L. Liu, *J. Electrochem. Soc.*, 2007, **154**, B201–B206.
5 A. Atkinson, S. Barnett, R. J. Gorte, J. T. S. Irvine, A. J. McEvoy, M. Mogensen, S. C. Singhal and J. Vohs, *Nat. Mater.*, 2004, **3**, 17–27.
6 X. F. Sun, S. R. Wang, Z. R. Wang, X. F. Ye, T. Wen and F. Q. Huang, *J. Power Sources*, 2008, **183**, 114–117.
7 C. Périllat-Merceroz, G. Gauthier, P. Roussel, M. Huvé, P. Gélin and R. N. Vannier, *Chem. Mater.*, 2011, **23**, 1539–1550.
8 M. C. Verbraeken, B. Iwanschitz, A. MaiAndreas and J. T. S. Irvine, *J. Electrochem. Soc.*, 2012, **159**, F757–F762.
9 X. Li, H. L. Zhao, N. S. Xu, X. Zhou, C. J. Zhang and N. Chen, *Int. J. Hydrogen Energy*, 2009, **34**, 6407–6414.
10 D. N. Miller and J. T. S. Irvine, *J. Power Sources*, 2011, **196**, 7323–7327.
11 E. Iglesia, *Appl. Catal., A*, 1997, **161**, 59–78.
12 S. K. Mohapatra, S. U. Sonavane, R. V. Jayaram and P. Selvam, *Tetrahedron Lett.*, 2002, **43**, 8527–8529.
13 C. Ando, H. Kurokawa and H. Miura, *Appl. Catal., A*, 1999, **185**, L181–L183.
14 X. Li, H. Zhao, F. Gao, Z. Zhu, N. Chen and W. Shen, *Solid State Ionics*, 2008, **179**, 1588–1592.

15 R. J. Gorte and J. M. Vohs, *Curr. Opin. Colloid Interface Sci.*, 2009, **14**, 236–244.
16 S. P. Jiang, *Int. J. Hydrogen Energy*, 2012, **37**, 449–470.
17 K. F. Chen, N. Ai, C. Lievens, J. Love and S. P. Jiang, *Electrochem. Commun.*, 2012, **23**, 129–132.
18 W. Kobsiriphat, B. D. Madsen, Y. Wang, L. D. Marks and S. A. Barnett, *Solid State Ionics*, 2009, **180**, 257–264.
19 B. D. Madsen, W. Kobsiriphat, Y. Wang, L. D. Marks and S. A. Barnett, *J. Power Sources*, 2007, **166**, 64–67.
20 W. Kobsiriphat, B. D. Madsen, Y. Wang, M. Shah, L. D. Marks and S. A. Barnett, *J. Electrochem. Soc.*, 2010, **157**, B279–B284.
21 L. Adijanto, P. V. Balaji, R. Kungas, R. J. Gorte and J. M. Vohs, *J. Mater. Chem.*, 2012, **22**, 11396–11402.
22 F. Guo, H. G. Zheng, Z. P. Yang and Y. T. Qian, *Mater. Lett.*, 2002, **56**, 906–909.
23 S. Q. Hui and A. PetricAnthony, *Mater. Res. Bull.*, 2002, **37**, 1215–1231.
24 L. M. Yang, L. Jonghe, C. P. Jacobsen and S. J. Visco, *J. Electrochem. Soc.*, 2007, **154**, B949–B955.
25 M. Roushanafshar, J. L. Luo, A. L. Vincent, K. T. Chuang and A. R. Sanger, *Int. J. Hydrogen Energy*, 2012, **37**, 7762–7770.
26 A. L. Vincent, J. L. Luo, K. T. Chuang and A. R. Sanger, *Appl. Catal., B*, 2011, **106**, 114–122.
27 J. H. Li, X. Z. Fu, J. L. Luo, K. T. Chuang and A. R. Sanger, *J. Power Sources*, 2012, **213**, 69–77.
28 S. Malo and A. Maignan, *Inorg. Chem.*, 2004, **43**, 8169–8175.
29 M. Y. Gong, X. B. Liu, J. Trembly and C. Johnson, *J. Power Sources*, 2007, **168**, 289–298.